To be published in Applied Optics:

Title:	Navy Prototype Optical Interferometer observations of geosynchronous satellite
Authors:	Robert Hindsley, J. Armstrong, Henrique Schmitt, Jonathan Andrews, Sergio Restaino, Christopher Wilcox, Frederick Vrba, James Benson, Michael DiVittorio, Donald Hutter, Paul Shankland, and Steven Gregory
Accepted:	23 January 2011
Posted:	10 February 2011
Doc. ID:	139423

Report Documentation Page

Form Approved
OMB No. 0704-0188

1. REPORT DATE	2. REPORT TYPE	3. DATES COVERED
JAN 2011		**00-00-2011 to 00-00-2011**

4. TITLE AND SUBTITLE	5a. CONTRACT NUMBER
Navy Prototype Optical Interferometer observations of geosynchronous satellite	5b. GRANT NUMBER
	5c. PROGRAM ELEMENT NUMBER
6. AUTHOR(S)	5d. PROJECT NUMBER
	5e. TASK NUMBER
	5f. WORK UNIT NUMBER
7. PERFORMING ORGANIZATION NAME(S) AND ADDRESS(ES) **Naval Research Laboratory,Remote Sensing Division,4555 Overlook Avenue NW,Washington,DC,20375**	8. PERFORMING ORGANIZATION REPORT NUMBER
9. SPONSORING/MONITORING AGENCY NAME(S) AND ADDRESS(ES)	10. SPONSOR/MONITOR'S ACRONYM(S)
	11. SPONSOR/MONITOR'S REPORT NUMBER(S)

12. DISTRIBUTION/AVAILABILITY STATEMENT
Approved for public release; distribution unlimited

13. SUPPLEMENTARY NOTES

14. ABSTRACT

15. SUBJECT TERMS

16. SECURITY CLASSIFICATION OF:			17. LIMITATION OF ABSTRACT	18. NUMBER OF PAGES	19a. NAME OF RESPONSIBLE PERSON
a. REPORT **unclassified**	b. ABSTRACT **unclassified**	c. THIS PAGE **unclassified**	**Same as Report (SAR)**	**26**	

Navy Prototype Optical Interferometer observations of geosynchronous satellites

Robert B. Hindsley,[1,*] J. Thomas Armstrong,[1] Henrique R. Schmitt,[1,2] Jonathan R. Andrews,[3] Sergio R. Restaino,[3] Christopher C. Wilcox,[3] Frederick J. Vrba,[4] James A. Benson,[4] Michael E. DiVittorio,[4] Donald J. Hutter,[4] Paul D. Shankland[4] Steven A. Gregory[5]

[1] *Remote Sensing Division, Naval Research Laboratory, 4555 Overlook Avenue NW, Washington, D.C. 20375, USA*

[2] *Computational Physics, Inc., 8001 Braddock Road, Suite 210, Springfield, VA 22151, USA*

[3] *Remote Sensing Division, Naval Research Laboratory, Kirtland AFB, Albuquerque, NM 87117, USA*

[4] *US Naval Observatory, Flagstaff Station, 10391 West Naval Observatory Road, Flagstaff, AZ 86001, USA*

[5] *Boeing LTS, 3550 Aberdeen Avenue, Kirtland AFB, Albuquerque, NM 87117, USA*

[*] *Corresponding author: hindsley@nrl.navy.mil*

Using a 15.9 m baseline at the Navy Prototype Optical Interferometer (NPOI), we have successfully detected interferometric fringes in observations of the geostationary satellite DirecTV 9S while it glinted on two nights in March 2009. The fringe visibilities can be fitted by a model consisting of two components, one resolved ($\gtrsim 3.7$ m) and one unresolved (~ 1.1 m). Both the length of the glint and the specular albedos are consistent with the notion that the glinting surfaces are not completely flat, and scatter reflected sunlight into an opening angle of roughly 15°. Enhancements to the NPOI that would improve geosat observations include adding an infrared capability, which could extend the glint season; and adding larger, adaptive-optics equipped telescopes. Future work may test the feasibility of observing geosats with aperture-masked large telescopes and of developing an array of six to nine elements.

OCIS codes: 100.3175, 110.3175, 120.3180.

1. Introduction

Direct imaging of geosynchronous satellites (geosats) would often be desirable in diagnosing problems with these satellites. For example, the geosat Galaxy 15 stopped responding to ground commands in April 2010. Imaging of this satellite might shed some light on the problem. Unfortunately, direct imaging of geosats is not possible with existing instruments. With 1 meter subtending 5 milliarcseconds (mas) at the altitude of a geosat, even the largest optical telescopes can barely resolve them.

Higher resolution is available using optical or infrared interferometers such as the Navy

Prototype Optical Interferometer [1] (NPOI), the Very Large Telescope Interferometer [2], or the CHARA array [3]. These interferometers can measure diameters of stars, with most stars visible to the naked eye having angular diameters of a few mas or less. But these interferometers, optimized for observing stars, typically have too MUCH resolution, and baselines too long, to image geosats. Objects whose angular size exceeds $\sim \lambda/B$, where λ is the observing wavelength and B is the baseline length, are resolved out: they produce fringes that become too weak to detect.

An additional problem in imaging geosats using interferometers is that the geosats are not very bright. Typically these have a visual magnitude of 10–14, depending on size and albedo of materials, distance, and illumination phase angle. Interferometers have to sense the atmospheric phase distortion and correct for it at millisecond time scales, and faint stars do not provide enough photons to sense the distortion before it changes. Increasing the size of the apertures on an array may not help if the aperture is larger than the turbulence scale length (r_0). For large apertures the light is no longer coherent unless adaptive optics are used to remove the phase distortion between turbulent cells. The use of adaptive optics requires siphoning off some of the light gained by using larger apertures. Because this loss of light may be appreciable, some have believed that the use of interferometers to directly image geosats is impossible.

There is one way around the faintness problem. Glints, or specular reflections of sunlight, from the spacecraft bus or solar panels may occur when the sun's declination is equal to that of the satellite. There are reports in the amateur community that geosats occasionally have become visible to the naked eye for a few minutes during these glints. To demonstrate the possibilities presented by optical interferometry, we used the NPOI in an attempt to detect

fringes from a geosat during a glint. Detecting fringes is the first step towards making an image, and fringe detection can be done with a single short baseline. Section 2 describes the instrument, and Section 3 describes the geosats. Section 4 presents the observations, which are discussed and interpreted in Sections 5 and 6. Section 7 discusses plans for further work, and we present conclusions in Section 8.

2. The NPOI

The NPOI is a collaborative effort of the US Naval Observatory, the Naval Research Laboratory, and Lowell Observatory. It is located about 19 km southeast of Flagstaff, Arizona, on Anderson Mesa. The array has three arms 120° apart, with arms running north, southeast, and southwest. While eventually the NPOI will have baselines as long as 437 m, at the time of these observations the longest baseline was 79 m. Currently, the NPOI observes in 16 channels spanning 550–850 nm in wavelength. Data taken at the long-wavelength end of this range samples source structure at lower resolution, while data at shorter wavelengths samples higher resolution.

The NPOI attempts to maintain zero delay difference among paths by employing a delay line for each siderostat. When the path lengths are equal, the NPOI is seeing the central fringe of the interferogram. To ensure that the fringe is in fact the central fringe, the delay lines dither around the expected position of the central fringe, producing an estimate of the fringe position (and delay mismatch) every 2 ms. Having enough photons to make a reliable estimate of the central fringe position at 500 Hz sets the faint magnitude limit for NPOI observations, which is about magnitude 6.5 in the Johnson R filter on the best nights. Fringes are unacceptably noisy for fainter stars.

When the central fringe is found, the NPOI control system attempts to track it. If fringe lock is lost, data collection halts until the fringe is found again. A data collection scan is finished when 30 s of data have been taken while fringe tracking; for stellar observations these 30 s of data must be obtained within a dwell time of 90 s. This limit is set by memory constraints in the data collection system. A more-detailed description of the NPOI can be found in [1].

3. Geosats and Glints

Communications geosats come in a variety of bus and solar panel configurations. Detailed information on satellite configurations is not generally available—presumably it is proprietary—and pictures are rarely available. Limited information is often available on the manufacturer's website, but usually the most detailed information comes from the websites of amateur satellite buffs. These sites can have an impressive amount of information, but often it is vague, and in any case it must be cross-checked.

DirecTV-9S is typical of one type of geostationary telecommunications satellites, with long, narrow solar panel arrays extending from either side of a central bus. It is a Space Systems/Loral LS-1300 spacecraft with a 7.5 m $\times$ 2.9 m $\times$ 3.3 m central bus and with solar panel arrays $\sim$ 2 m wide spanning a total of 31 m. These dimensions correspond to 43 mas $\times$ 17 mas $\times$ 19 mas for the bus and 12 mas $\times$ 180 mas for the solar panel arrays as seen from the ground. (1 milliarcsecond [mas] = 0.001 arc sec = 5 nrad.) The solar panels are oriented north–south as in all satellites of this type, with the normal to the panels pointing approximately toward the Sun. At the beginning of the spacecraft's life, when the panels are very efficient, the panels are rotated about their long axis to decrease

the power generated. A sketch of DirecTV-9S is shown in Figure 1. This sketch is taken from a document by Arianespace (`http://www.arianespace.com/images/launch-kits/launch-kit-pdf-eng/06_oct_13.pdf`), which launched the satellite. The identical sketch (even with identical background) is available on the Loral website (`http://www.ssloral.com/images/products/renderings/DirecT_VIIS.jpg`), but is said to represent DirecTV-7S, which has the same type of bus as DirecTV-9S.

With the NPOI situated at latitude 35°N, geosynchronous satellites are seen at a declination of −5.6°. The two NPOI glint seasons occur when the Sun has the same declination, and are centered on March 1 and October 10, lasting about a week. For an individual satellite the time of a glint, if it occurs, depends on its azimuth and the relative orientation of the solar panels. If the panels are pointed directly at the sun, the glint is seen when the sun's azimuth (below the horizon, of course) is opposite to that of the satellite, which is also the time at which the satellite may pass through the earth's shadow. From the latitude of the NPOI, these passes through the shadow occur at end of the March glint season and the beginning of the October season.

We restrict NPOI observations to elevations greater than 40°. The geosats have a maximum elevation of about 49° as seen from Flagstaff. As a result, we observed satellites no more than 30° off the meridian. One result is that baseline foreshortening is mostly due to the north–south extent of the baselines, which in the case of these observations is small.

4. Observations

As noted in the Introduction, objects whose angular size exceeds $\sim \lambda/B$ produce weak or undetectable fringes. For our observations, the shortest available baseline length $B = 15.9$ m.

With a central wavelength $\lambda = 700$ nm, $\lambda/B \sim 9$ mas, corresponding to ~ 1.6 m on orbit, i.e., just small enough to encourage us to attempt to detect a geosat.

Observations were attempted on several satellites during 11–17 October 2007 , 27 February–4 March 2008, 8–16 October 2008, and 26 Feb–4 March 2009 (all dates are UTC). We used three NPOI array elements, labeled E6, AE, and AC, that produce baseline lengths and orientations 15.9 m long at azimuth $-68°$ and 18.9 m at 93° for the E6–AE and AE–AC pairs, respectively. (See [1] for details of the NPOI layout.) No data were taken on the E6–AC baseline, so no closure phase information was available. Because the shortest of these baselines, E6–AE, is nearly east–west, it exhibits almost no foreshortening during geosat observations.

The observations for this study differ from typical NPOI stellar observations in several respects. Diurnal delay tracking, needed for stars, is not needed for satellites. The normal dwell-time limit of 90 s, after which a target star is dropped and the observing sequence proceeds to the next target, was also not implemented. Instead, data collection was attempted until the satellite became too faint, as judged by the signal in the narrow-angle trackers. Alternating target observations with a fringe-visibility calibration star was turned off as well; for these observations, we observed only the target while it was bright enough for fringe detection. We observed a calibrator star immediately after any target that exhibited even a hint of detected fringes.

The main difficulty in observing geosats with the NPOI concerns knowing the satellite's apparent position on the sky as viewed from the NPOI. The central fringe must be found before it can be tracked. The position of the satellite—expressed in horizon coordinates, azimuth and elevation—is a significant source of error in predicting the proper positioning

of the delay lines; a 1 arcsec error in the satellite position is equivalent to having the delay line out of position by 300 μm. It takes several minutes to search through that much delay space, which is roughly the length of time the geosat is brighter than the $R \sim 6$ limit and can be tracked. Setting the delay lines within 300 μm, equivalent to knowing the position to better than 1 arcsec, is vital for success.

The commonly available satellite orbit parameters, known as Two Line Elements (TLEs), do not yield positions nearly so precise as 1 arcsec. While the NPOI star acquisition system can easily find the satellites and steer the light through the system, sub-arcsecond position determination from siderostat pointing parameters is currently unavailable at the NPOI.

We used the 1-meter Ritchey-Chrétien telescope of the US Naval Observatory's Flagstaff Station (USNOFS) to measure the satellite positions and to monitor the magnitude of the satellite. Images were obtained on a 2048^2 CCD with 0.68 arcsec/pixel using an $R_{\rm C}$ filter in the Cousins system. This gave a field of view, 23 arcmin wide, that could include as many as four geosats. To determine which satellite was the target, we used the commercially available program The Sky (Software Bisque, Inc., Golden, CO `http://www.bisque.com`). The telescope tracking was turned off, so that the satellites were stationary on the CCD while star images were trailed. This procedure meant that increasing the exposure time did not add reference stars for the astrometric solution; the stellar images simply became longer tracks. The exposure time ranged from 0.8 s to 5 s and was set by the brightness of the satellite. These photometric data are of sufficient quality to permit analysis of the orientation and flatness of the solar panels [4].

Astrometric solutions were performed using software developed for these observations, including a modified version of the Spacewatch software supplied by Dr. Jeff Larsen of

the US Naval Academy. The Naval Observatory Vector Astrometry Subroutines (NOVAS) package [5] was used to perform frame transformations and to include apparent position effects such as aberration and polar motion. A parallax correction had to be applied to all positions due to the 19 km distance (roughly due east) from the USNOFS site to the NPOI site.

Positions were measured starting as much as an hour before the glint maximum. These satellites are all classified as geostationary, meaning that not only are they geosynchronous (period matching the Earth's rotation), but also that these satellites are actively station-keeping and thus maintain inclinations close to zero with respect to the celestial equator as well as eccentricities close to zero. In practice, the inclinations are kept within 0.1° of the equator. Our experience was that position changes of 0.5 arcsec/minute each in altitude and azimuth were not unusual.

Geosats saturated the USNOFS camera at $R_{\rm C} \sim 7$; once the images became saturated, reliable position measurements could not be obtained. In effect no positions could be obtained for about 20 min before glint maximum, and the positions based on unsaturated images had to be extrapolated to the time of glint maximum. Observing with the USNOFS 1 m telescope did continue through the maximum in order to obtain magnitude estimates. Switching to an Hα filter gave unsaturated images farther into the glint, and these magnitudes were easily transformed to a scale consistent with the $R_{\rm C}$ measurements. However, there were not enough reference stars in these fields to do an astrometric solution with the Hα filter, and in any case the Hα images also saturated at about $R_{\rm C} \sim 5$.

5. Results

Neither autumn observing session produced any successful fringe measurements. On two different occasions, 28 February and 1 March 2008, the data seemed to exhibit fringe-tracking success for periods of about 1 s on the E6–AE baseline while observing DirecTV-9S, resulting in a tentative detection [6]. No observation of DirecTV-9S could be performed in October 2008 as the satellite did not glint brightly enough.

On 2 March 2009 at 0532 UTC (local time 2232 MST, 01 March 2009), we again detected fringes while observing DirecTV-9S, but with significantly better signal-to-noise ratio than the previous year. Fringes were detected on the E6–AE baseline, but not on the slightly longer AE–AC baseline. DirecTV-9S, located at a longitude of 101°W, was at an elevation of 47.8° and azimuth of 161.8° as seen from the NPOI. A second successful detection of DirecTV-9S followed on 3 March 2009. The observed visibilities from these two nights, shown in Fig. 2, are the results we will discuss below.

As a check on the validity of the 2009 detections, we calculated power spectra of the fringe frequency during the 2 ms dither cycle. Given the backend setup for these observations, the spectra should show power at a frequency $f = 3$, where f is measured in fringes per dither stroke length. The power spectra for two 1 s frames, one from each date, are shown in Fig. 3.

For comparison, we also show the calibrated visibilities and a fringe power spectrum from the 2008 tentative detection in Fig. 4. The visibilities in the blue channels are very noisy, providing no useful information shortward of λ600 nm, and the power spectrum shows little power at $f = 2$, the fringe frequency expected for that night's backend setup. Although the 2008 detection was weak, the 2009 detections strengthen the case for its having been real.

6. Discussion

Clearly we cannot make an image from data taken on only one baseline. However, we can make some inferences about the size of the glinting area from the fringe visibilities V and their dependence on wavelength λ. Combining size and brightness information also allows us to calculate specular albedos, the fraction of incident light that is specularly reflected. This is the sense in which we will use albedo throughout.

The low visibilities seen in our March 2009 results (Fig. 2) could indicate a single resolved component; however, the relative flatness of V as a function of increasing λ (i.e., of decreasing resolution) does not fit such a model. We have fitted a more complex model—two uniformly-bright circular components with diameters L_1 and L_2—to the data. In these fits, the two components contribute roughly equal amounts of the flux. However, they are significantly different in size, so their contributions to the fringe visibility are quite different. The larger component is resolved, i.e., its contribution to the visibility is very small, so its primary effect is to dilute the visibility of the smaller component.

We found two equally good solutions for each night, in which the two components contribute roughly equal amounts of flux but the fringe visibility of the larger component is small. The primary difference between the two is that L_2, the size of the larger, resolved component, is ≈ 3.6 m in one of the fits and ≈ 7 m in the other. The parameters of these fits are given in Table 1. The first two columns list the diameters L_1 and L_2 of the components; the third lists the ratio of the fluxes; the fourth gives the reduced χ^2 of the fit, and the fifth column lists the peak R magnitude for each night.

Figure 5 shows $V(\lambda)$ for the $L_2 = 7$ m model for 3 March 2009, along with the contributions

Table 1. Two-component model fits to March 2009 data

L_1 (m)	L_2 (m)	F_1/F_2	χ^2_ν	$m_{\rm R}$(peak) (mag)
2 March 2009:				2.4
1.3	7.0	0.59 / 0.41	1.3	
1.3	3.4	0.67 / 0.33	1.4	
3 March 2009:				< 1.5?
1.1	7.2	0.47 / 0.53	0.8	
1.2	3.7	0.56 / 0.44	0.8	

each component makes to $V(\lambda)$. The 2 March 2009 fits show similar results, the primary difference being that on 2 March the satellite was ~ 1 mag (a factor of ~ 2.5) fainter. Both components appear to have brightened from 2 March to 3 March. The model fits suggest that the resolved component brightened by a factor of ~ 3, while the unresolved component brightened by a factor of ~ 2.

The ambiguity between best-fit solutions with differing values of L_2 can be understood by considering the visibilities $V(\lambda)$ of this component. We are seeing either the second null (for $L_2 \approx 3.6\ m$) or the fourth null (for $L_2 \approx 7$ m) of the $V(\lambda)$ curve, and in both cases, the visibility follows the same trend: slightly negative for $\lambda \gtrsim 700$ nm and slightly positive for $\lambda \lesssim 700$ nm. Figure 5 illustrates this behavior. This ambiguity highlights the fact that these models are not unique fits to the data.

It is important to keep in mind that the baseline on which we made the detection is

sensitive only to the east-west extent of the satellite. We have no information on the north-south extent of either component. Nevertheless, although these models are not definitive, they do make a case for the glint being due to two separate structures.

With these fits in mind, we returned to the 2008 detection, to which we had earlier fit a single-component model. We find that the 2008 data are consistent with two-component models similar to the 2009 models. Because the 2008 data have considerably lower signal-to-noise ratio, the most we can conclude is that the glinting areas for the two years are roughly similar.

Are the albedos implied by our model plausible? As Schaefer et al. [7] have pointed out, the expected brightness of a glint, which is a reflection of a portion of the Sun's surface, can be estimated from the angular size of the satellite and an assumed albedo. In our case, we have a measured brightness from the USNOFS observations and an angular size from the NPOI, so we can invert the calculation: given the glint magnitude m, the albedo A is given by the ratio of angular sizes of the Sun and the satellite times the ratio of their fluxes, or

$$A = \left(\frac{\theta_0}{L/H}\right)^2 10^{-0.4(m-m_0)}, \tag{1}$$

where θ_0 is the angular diameter of the Sun (0.0094 rad), H is the distance to the satellite (about 35700 km for a geosat), L is the diameter of the glinting region, assumed to be circular, and m_0 is the Sun's apparent magnitude (-27.1 in the R_C filter), from $m(V)_\odot = 26.75$ [8] and $(V - R_\mathrm{C})_\odot = 0.354$ [9]. (Schaefer et al. [7] implicitly assume a rectangular glinting region of angular size L/H and use the solar radius rather than the diameter, accounting for a difference of a factor of π between their expression and ours.)

Because our model has two components, it is necessary to split the albedo calculation in

two. First consider the model with $L_2 = 7$ m fit to the 2 March 2009 data, on which the satellite peaked at $R_C = 2.5$. For this case, the brighter component has 59% of the flux. The inferred albedos are 0.0015 and 0.064 for the resolved (7 m) and unresolved (1.3 m) components, respectively. For 3 March 2009, assuming that the satellite peaked at $R_C = 1.5$ (although it may have been brighter), we find albedos of 0.0042 and 0.15 for the 7.2 m and 1.1 m components. Using the smaller values of L_2 increases the albedo of the resolved component to 0.005 for 2 March (while increasing the albedo of the unresolved component slightly, to 0.067); for 3 March, the albedo of the resolved component increases to 0.013, while the albedo for the unresolved component remains unchanged.

The albedos of the resolved component seem impossibly small. One possible explanation is that this component may be small in the north-south direction, along which our observations do not offer any size information, rather than being circular as we assume. But it would have to be very narrow to account for the small albedo.

However, the length of the glints observed on these two nights [4] offers another explanation. It is very probable that the glinting surfaces are not completely flat, so the reflected sunlight is spread into a wide opening angle. A glint from an ideal satellite with a perfectly flat reflecting surface has an opening angle of $0.^{\circ}5$ (one solar diameter) and would last 2 minutes. In actuality, the DirecTV-9S glints in 2009 lasted up to an hour, with a gradual rise and fall, suggesting an opening angle of $\sim 15^{\circ}$.

This possibility is supported by the peak brightness of the glints. For an ideal satellite the size of DirecTV-9S (11 mas $\times$ 165 mas), the glint would peak at $R_C \approx -4.3$ mag. In actuality, on 2 and 3 March, respectively, it peaked at +2.5 mag and at +1.5 mag or brighter, i.e., ~ 500 times and ~ 300 times fainter, roughly consistent with an opening angle of $\sim 15^{\circ}$. The

albedos of the unresolved component, 0.06 and 0.16 for the two nights, are also somewhat low, which is also probably due to the reflecting surface not being entirely flat.

In addition to DirecTV-9S, we observed glints from several other satellites, but did not detect interference fringes. In March 2009, each USNOFS DirecTV-9S frame included three other satellites, GE-2 and GE-4 to the east of DirecTV-9S, and DirecTV-4S to the west. GE-2 and DirecTV-4S glinted, but our attempts to find fringes with the NPOI were somewhat cursory; the primary effort was focused on DirecTV-9S. We were also unsuccessful in finding fringes from several other satellites that glinted at times when DirecTV-9S was not glinting. It is likely that the seeing and transparency were degraded when observing was concentrated on the other satellites.

But it is also possible that there was some quirk of the DirecTV-9S spacecraft bus and general configuration that was responsible for the success with that particular satellite. The two components of our model may represent particular components not present on other geosats. We gathered what information we could from other DirecTV satellites on the supposition that they would be more likely to share the configuration of DirecTV-9S. The only other DirectTV geosat using the same bus, and with the suffix **S** for spot beam (implying a specific dish arrangement), is DirecTV-7S, at azimuth 192.°6 and elevation 48.°6 from NPOI. Only on the final night of the observing run were we able to attempt observations of this satellite. Fringe tracking was not achieved, quite possibly due to transparency and seeing that were noticeably less than optimal.

7. Future Possibilities

The NPOI, being designed and normally utilized for observing stars, is not optimized for geosat observations. However, the instrument was designed to be reconfigurable; some of the siderostats can be relocated to any one of ten fixed stations on each arm. Although this capability has been little utilized, due to the as-yet-incomplete implementation of imaging siderostats, a three-element array with suitably small baselines could be set up and closure phase obtained. This array would not produce an image, but it would be a significant next step.

To explore the minimal requirements for producing an image, consider the simulated noiseless interferometer images shown in Fig. 6. While these simulations were not done with the NPOI configurations, they indicate that six siderostats can produce an image suitable for determining whether the solar arrays have deployed (Fig. 6b), although spurious bright spots appear on the spacecraft bus. The nine-element configuration does better at imaging structures on the bus (Fig. 6c). However, the improvement in going from nine siderostats to twelve (Fig. 6d) is less noticeable. This last result is consistent with Perley [10], who found that image quality improves more slowly as the number of interferometer elements rises beyond ~ 10.

Unfortunately, the NPOI, with only six delay lines, cannot combine the light from more than six siderostats at a time, and increasing that number would be prohibitivly expensive. Some of the benefits of a nine-element array could be achieved at the NPOI by combining light from six siderostats at a time, although during the few available minutes during which a geosat glints brightly enough for fringe tracking, only one or two such reconfiguations

(resulting in observations using two or three subarrays) would be possible.

Enhancements that would permit geosat imaging throughout the year at the NPOI, rather than just during two limited glint seasons, are equally as important and are simpler and less expensive to implement. The simplest improvement would be to add an observing capability in the near IR, such as the K band at 2.2 μm. At those wavelengths the albedo of the spacecraft is higher. More importantly, the atmosphere has a longer coherence time t_0 and turbulence scale length r_0. The former allows longer integrations, while the latter means that there is more coherence across the aperture than there would be in the optical. This combination greatly relaxes the requirements on an adaptive optics system. Adaptive optics systems (see [11]) coupled with the 1.4 m and 1.8 m telescopes being considered for the NPOI could extend the NPOI capabilities enough to observe geosats year round.

Finally, the relatively short baseline length ($\sim$ 10 m) that is needed to resolve the larger-scale structures of a geosat could also be obtained by aperture masking observations on a telescope with an aperture large enough to provide such baselines. Aperture masking techniques could sample many baselines simultaneously. One particular example is the Large Binocular Telescope (LBT), consisting of two mirrors 8.4 m in diameter on one mount, with centers separated by 14.4 m.

8. Conclusion

We have made a first step towards imaging geosats via interferometry by successfully measuring interferometric fringes from the glinting geostationary satellite DirecTV-9S on two nights in March 2009. The calibrated visibilities can be fitted by a model consisting of an unresolved component 1 to 2 m in size and a resolved component $\gtrsim$ 3.7 m in size. The

two components contribute roughly equal shares of the total flux.

Future observations at the NPOI would benefit from shorter baselines and/or the addition of an infrared detector. Both of these enhancements would make it easier to observe with multiple baselines, which will be needed for true imaging of these satellites. Larger, adaptive-optics equipped apertures, such as the 1.4 m and 1.8 m telescopes being considered for the NPOI, could make it possible to image geosats outside the glint seasons.

Acknowledgements

The authors gratefully acknowledge the engineering staff of the US Naval Observatory–Flagstaff Station for supporting observations on various telescopes, especially the 1 m Ritchey-Chrétien telescope. Thanks also to Mr. Len Bright and Dr. Ted Dunham of Lowell Observatory for help with supporting observations using the Hall Telescope at the Lowell Observatory dark site on Anderson Mesa.

References

[1] J. T. Armstrong, D. Mozurkewich, L. J Rickard, D. J. Hutter, J. A. Benson, P. F. Bowers, N. M. Elias II, C. A. Hummel, K. J. Johnston, D. F. Buscher, J. H. Clark III, L. Ha, L.-C. Ling, N. M. White, and R. S. Simon, "The Navy Prototype Optical Interferometer," Astrophys. J. **496**, 550–571 (1998).

[2] A. Glindemann et al., "The VLTI – A Status Report," Astrophys. Space Sci. **286**, 35–44 (2003).

[3] T. A. ten Brummelaar, H. A. McAlister, S. T. Ridgway, W. G. Bagnuolo, Jr., N. H. Turner, L. Sturmann, J. Sturmann, D. H. Berger, C. E. Ogden, R. Cadman, W. I.

Hartkopf, C. H. Hopper, and M. A. Shure, "First Results from the CHARA Array. II. A Description of the Instrument," Astrophys. J. **628**, 453–465 (2006).

[4] F. J. Vrba, M. E. DiVittorio, R. B. Hindsley, H. R. Schmitt, J. T. Armstrong, P. D. Shankland, D. J. Hutter, and J. A. Benson, "A Survey of Geosynchronous Satellite Glints," in *Proceedings of the Advanced Maui Optical and Space Surveillance Technologies Conference,* S. Ryan, ed. (The Maui Development Board), p. E28 (2009).

[5] G. H. Kaplan, "NOVAS," Bull. Am. Astron. Soc. **22,** 930–931 (1990).

[6] J. T. Armstrong, R. B. Hindsley, S. R. Restaino, J. A. Benson, D. J. Hutter, F. J. Vrba, R. T. Zavala, S. A. Gregory, and H. R. Schmitt, "Observations of a Geosynchronous Satellite with Optical Interferometry," Proc. SPIE 7468, 74680K (2009).

[7] B. E. Schaefer, M. Barber, J. J. Brooks, A. Deforrest, P. D. Maley, N. W. McLeod III, R. McNiel, A. J. Noymer, A. K. Presnell, R. Schwartz, and S. Whitney, "The Perseus Flasher and Satellite Glints," Astrophys. J. **320,** 398–404 (1987).

[8] A. N. Cox, *Allen's Astrophysical Quantities*, Fourth Ed. (The Athlone Press, 2000), §14.1.4.

[9] J. Holmberg, C. Flynn, and L. Portinari, "The colours of the Sun," Mon. Not. R. Astron. Soc. **367,** 449–453 (2006).

[10] R. Perley, "The 'New Mexico Array' Preliminary Configuration and Imaging Performance Studies," presented at the EVLA Phase II Definition Meeting, Socorro, New Mexico, 23–25 Aug. 2001, http://www.aoc.nrao.edu/evla/geninfo/meetings/evla2plan/ .

[11] S. R. Restaino, T. Martinez, J. R. Andrews, C. C. Wilcox, F. Santiago, and D. M. Payne, "The Naval Research Laboratory MEM adaptive optics program," Proc. SPIE

7209, 72090F (2009).

Fig. 1. Sketch of DirecTV-7S/9S from the Loral website. These satellites use the Loral FS 1300 Omega bus. The Loral website presents this picture as DirecTV-7S; an identical picture is presented as DirecTV-9S in a document by ArianeSpace, which launched the latter satellite.

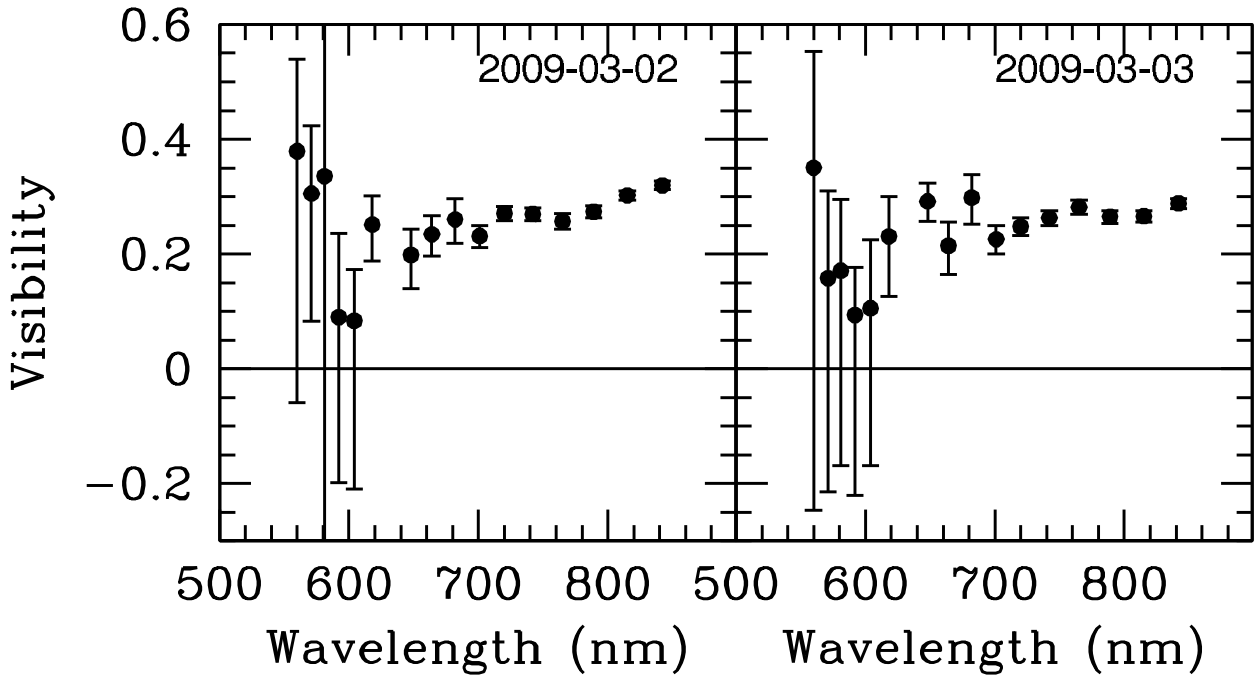

Fig. 2. Calibrated visibility as a function of wavelength for DirecTV-9S as observed on 2 and 3 March 2009.

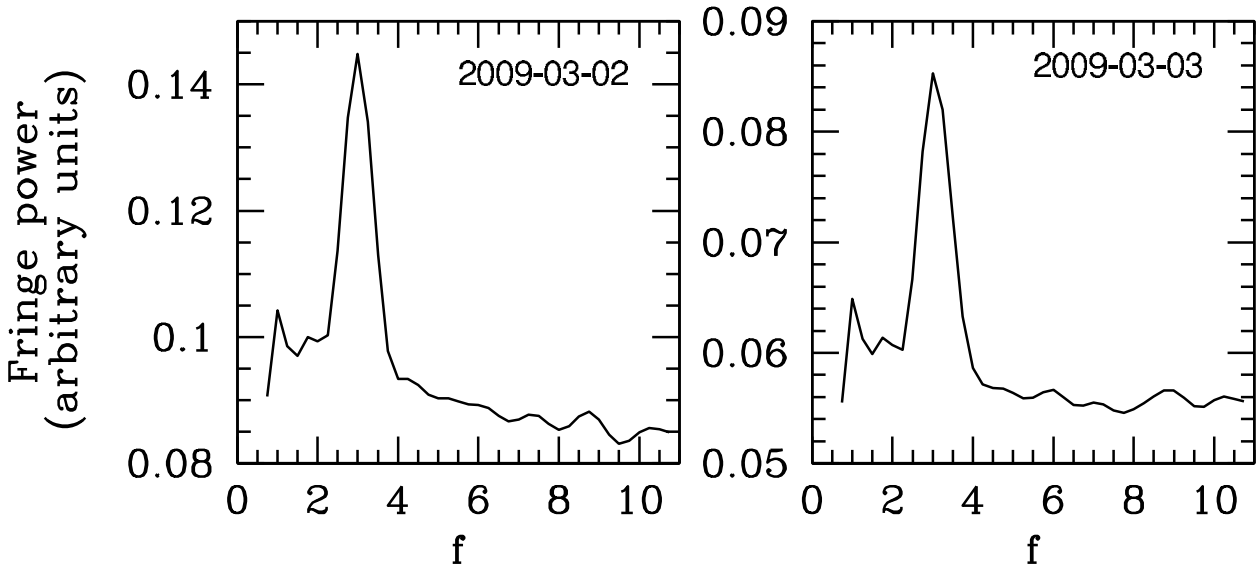

Fig. 3. Plot of fringe power as a function of fringe scanning frequency f for 1 second packets of fringe data for DirecTV-9S on 2 and 3 March 2009. The backend setup should result in a peak in fringe power at $f = 3$.

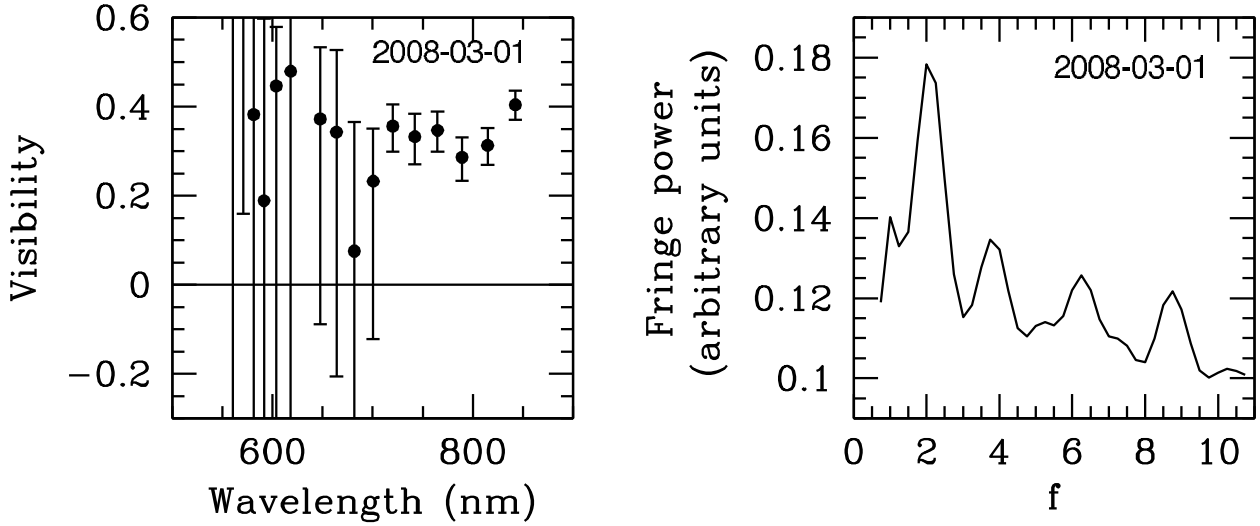

Fig. 4. DTV-9S calibrated visibilities as a function of wavelength (left) and fringe power as a function of fringe scanning frequency f (right) from 1 March 2008 data. The backend setup should result in a peak in fringe power at $f = 2$.

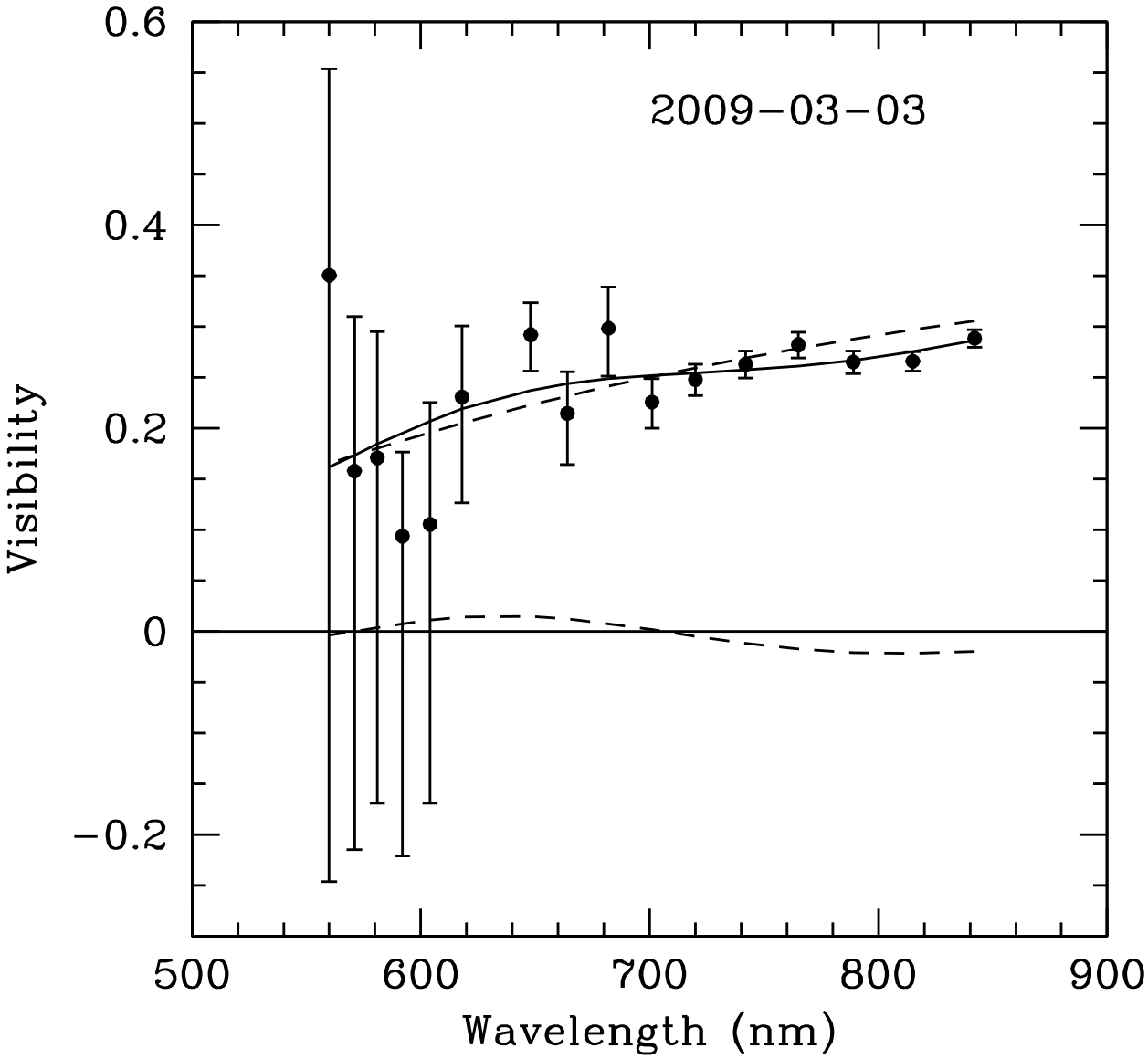

Fig. 5. Calibrated visibilities as a function of wavelength from 3 March 2009 data, and flux-scaled visibilities from a two-component model fit to the data. The dashed curves show the model visibilities multiplied by the fractional contribution of the flux. The model visibilities are those of the first of the 3 March 2009 models listed in Table 1. This model consists of a smaller circular component of size 1.1 m (6.2 mas at geostationary distance) with 46% of the flux (upper dashed curve) and a larger component of 7 m (40 mas) size with 54% of the flux (lower dashed curve). The solid curve is the sum of the dashed curves. The larger, resolved component has a visibility amplitude of almost

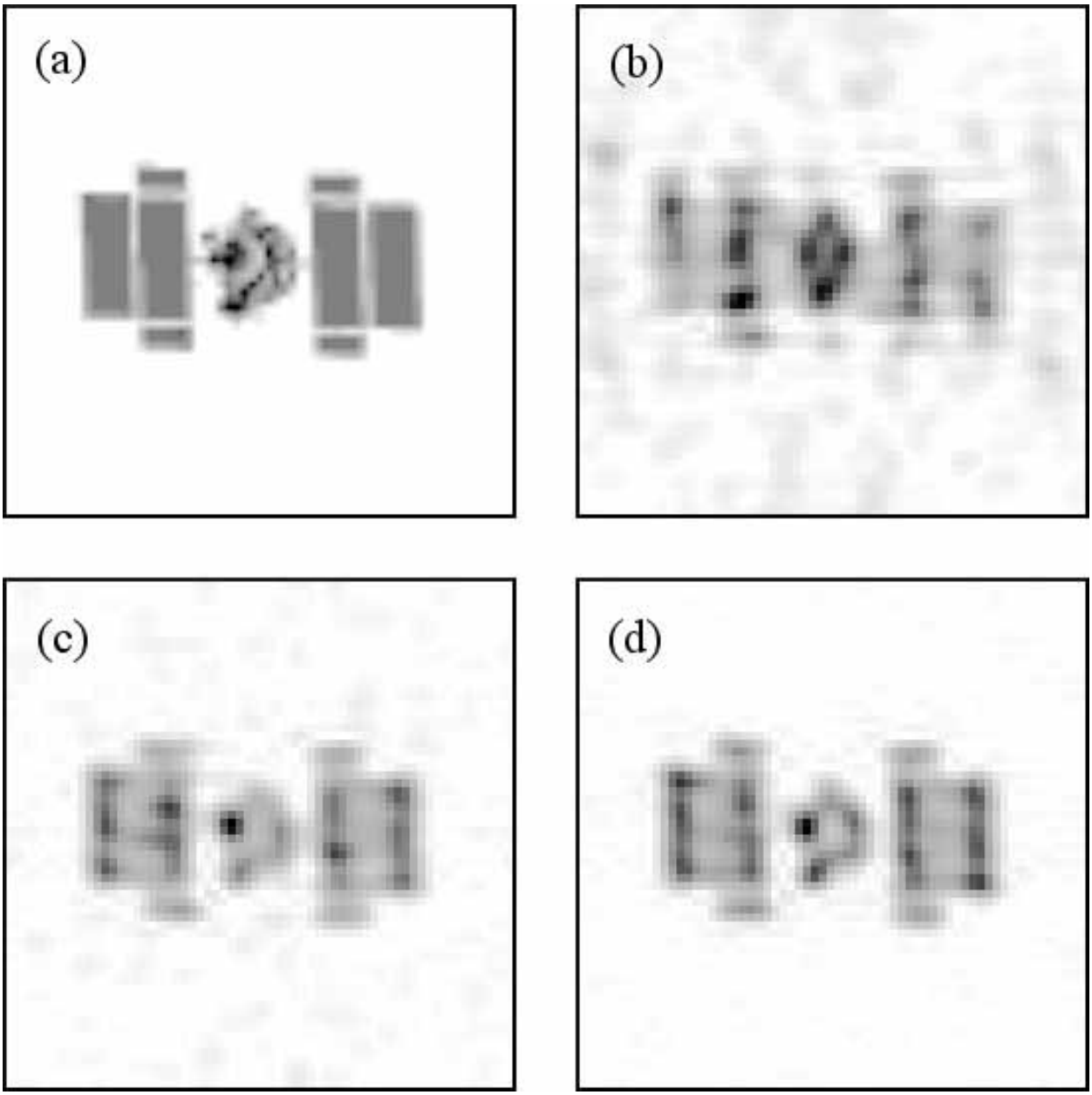

Fig. 6. Imaging simulation for six, nine, or twelve array elements. The truth image is shown in (a). The images in (b), (c), and (d) were reconstructed from noiseless simulations of observations with Y-shaped interferometer arrays using (b) six, (c) nine, or (d) twelve array elements.